Combined PARP1-Targeted Nuclear Contrast and Reflectance Contrast Enhance Confocal Microscopic Detection of Basal Cell Carcinoma

Aditi Sahu[1], Jose Cordero[1,2], Xiancheng Wu[1,3], Susanne Kossatz[4–6], Ucalene Harris[1], Paula Demetrio Desouza Franca[4], Nicholas R. Kurtansky[1], Niasia Everett[1], Stephen Dusza[1], Jilliana Monnier[1,7], Piyush Kumar[8], Christi Fox[9], Christian Brand[10], Sheryl Roberts[4], Kivanc Kose[1], William Phillips[1], Erica Lee[1], Chih-Shan Jason Chen[1], Anthony Rossi[1], Kishwer Nehal[1], Melissa Pulitzer[1], Caterina Longo[11,12], Allan Halpern[1], Thomas Reiner[4,13,14], Milind Rajadhyaksha*[1], and Manu Jain*[1]

[1]Dermatology Service, MSKCC, New York, New York; [2]Medical Sciences Campus, University of Puerto Rico, San Juan, Puerto Rico; [3]SUNY Upstate Medical University, Syracuse, New York; [4]Department of Radiology, MSKCC, New York, New York; [5]Department of Nuclear Medicine, University Hospital Klinikum Rechts der Isar and Central Institute for Translational Cancer Research, Technical University Munich, Munich, Germany; [6]Department of Chemistry, Technical University Munich, Munich, Germany; [7]Dermatology Department and Skin Cancer Department, La Timone Hospital, AP-HM, Aix-Marseille University, Marseille, France; [8]Department of Environmental Medicine and Public Health, Icahn School of Medicine at Mt. Sinai, New York, New York; [9]Caliber Imaging and Diagnostics, Rochester, New York; [10]Summit Biomedical Imaging, New York, New York; [11]Department of Dermatology, University of Modena and Reggio Emilia, Modena, Italy; [12]Azienda Unità Sanitaria Locale–IRCCS di Reggio Emilia, Centro Oncologico ad Alta Tecnologia Diagnostica-Dermatologia, Reggio Emilia, Italy; [13]Department of Radiology, Weill Cornell Medical College, New York, New York; and [14]Chemical Biology Program, MSKCC, New York, New York

Reflectance confocal microscopy (RCM) with endogenous backscattered contrast can noninvasively image basal cell carcinomas (BCCs) in skin. However, BCCs present with high nuclear density, and the relatively weak backscattering from nuclei imposes a fundamental limit on contrast, detectability, and diagnostic accuracy. We investigated PARPi-FL, an exogenous nuclear poly(adenosine diphosphate ribose) polymerase (PARP1)–targeted fluorescent contrast agent, and fluorescence confocal microscopy toward improving BCC diagnosis. **Methods:** We tested PARP1 expression in 95 BCC tissues using immunohistochemistry, followed by PARPi-FL staining in 32 fresh surgical BCC specimens. The diagnostic accuracy of PARPi-FL contrast was evaluated in 83 surgical specimens. The optimal parameters for permeability of PARPi-FL through intact skin was tested ex vivo on 5 human skin specimens and in vivo in 3 adult Yorkshire pigs. **Results:** We found significantly higher PARP1 expression and PARPi-FL binding in BCCs than in normal skin structures. Blinded reading of RCM–and–fluorescence confocal microscopy images by 2 experts demonstrated a higher diagnostic accuracy for BCCs with combined fluorescence and reflectance contrast than for RCM alone. Optimal parameters (time and concentration) for PARPi-FL transepidermal permeation through intact skin were successfully determined. **Conclusion:** Combined fluorescence and reflectance contrast may improve noninvasive BCC diagnosis with confocal microscopy.

Key Words: basal cell carcinoma; cancer diagnosis; reflectance confocal microscopy; nuclear contrast; fluorescence confocal microscopy; in vivo

J Nucl Med 2022; 63:912–918
DOI: 10.2967/jnumed.121.262600

Received May 18, 2021; revision accepted Aug. 26, 2021.
For correspondence or reprints, contact Manu Jain (jainm@mskcc.org).
*Contributed equally to this work.
Published online Oct. 14, 2021.

Basal cell carcinomas (BCCs) occur with high incidence rates of more than 4 million in the United States, Europe, and Australia every year (*1*). Diagnosis is based on dermoscopy followed by biopsy and histopathology. BCCs can manifest as superficial, nodular, infiltrative, and micronodular subtypes (*2*). Although dermoscopy provides high sensitivity (80%–100%), the specificity remains low and variable (32%–90%), particularly for lesions lacking distinct pigmentation or vascular patterns (so-called pink lesions) (*3–5*). This lower specificity leads to approximately 3–5 benign lesions being biopsied for every detected malignancy, which translates to roughly 12–15 million biopsies annually (*6*). The specificity for BCC diagnosis has recently been improved with reflectance confocal microscopy (RCM).

RCM is a noninvasive high-resolution, label-free, quasihistopathologic imaging technique that shows cellular-level morphology and architecture in skin to a depth of 200 μm (*7–9*). RCM is based on the detection of singly backscattered light from subsurface optical sections (*10–13*). RCM detects BCCs with sensitivity of 76%–94% and specificity of 54%–95% (*14–16*). When combined with dermoscopy, RCM provides approximately 50% higher specificity, with a resulting approximately 2-times drop in the benign-to-malignant biopsy ratio compared with dermoscopy alone (*17–19*). Although the use of RCM has improved diagnostic accuracy at the bedside, the backscattered contrast imposes a fundamental limit for BCC diagnosis. Because of weak backscatter from intranuclear chromatin, nucleus-dense BCCs appear dark relative to the surrounding dermis. But nucleus-dense normal structures (hair follicles, lower basal cell layer of epidermis) also appear dark, thus mimicking BCCs (*16,20*). This limitation may be overcome with an exogenous molecule-targeted fluorescence nuclear contrast agent and fluorescence confocal microscopy (FCM) imaging.

PARPi-FL is a newly developed small-molecular (620 Da), poly-(adenosine diphosphate ribose) polymerase (PARP1)–targeted

fluorescent reporter (*21*). PARPi-FL is BODIPY-FL (Molecular Probes) conjugated to the PARP inhibitor olaparib, possessing the strong PARP1 specificity of olaparib (*21,22*) and the strong fluorescence properties of BODIPY-FL, and has shown specific nuclear labeling and tumor imaging (*23,24*). The Food and Drug Administration accorded investigational-new-drug status to PARPi-FL, and a phase I/II trial is in progress (NCT03085147) for imaging oral cancers in patients (*25,26*). Higher intranuclear accumulation in tumors, rapid tissue permeation (4.6 μm/s (*27*)), safety, and detectability deeper in tissue makes PARPi-FL attractive for BCC diagnosis.

However, for in vivo use in patients, 2 central questions must be addressed: can the exogenous PARPi-FL nuclear contrast improve diagnostic accuracy for BCCs, and can PARPi-FL be quickly and effectively delivered transepidermally to BCCs in the dermis through intact skin? We report the results of our investigation on PARP1 expression, PARPi-FL staining, and permeability in this article (Fig. 1).

MATERIALS AND METHODS

Sample Collection

PARP1 expression was investigated on formalin-fixed, paraffin-embedded specimens. For experiments on PARPi-FL staining, surgically excised fresh discarded BCCs and normal specimens were collected after Mohs surgeries. For the permeability experiments, large (5 × 5 cm) specimens of normal breast skin were collected at the end of mastectomies. All samples were collected under various institutional review board–approved protocols.

PARP1 Expression in BCCs

Two adjacent thin (5 μm) formalin-fixed, paraffin-embedded sections were obtained for PARP1 immunohistochemistry and hematoxylin and eosin (H&E) staining. PARP1 immunohistochemistry was performed according to a previously described procedure (*24*). We used an anti-PARP1 rabbit monoclonal antibody (46D11; Cell Signaling Technology) at 0.4 μg/mL, followed by a biotinylated goat anti-rabbit IgG (PK6106; Vector Labs) at a 1:200 dilution.

Quantification of PARP1 Expression

Immunohistochemistry-stained and H&E-stained sections were digitally scanned (Aperio ScanScope Slide Scanner; Leica Biosystems). BCCs and surrounding normal structures—hair follicles, sebaceous glands, and epidermis—were annotated by a pathologist using different color codes. PARP1 was quantified using the Aperio Positive Pixel Count Algorithm (Leica Biosystems) (*28*). Thresholding was performed on the diaminobenzidine PARP1-positive area, and total area was determined by hematoxylin-stained area. PARP1 positivity (integrated positive pixel area/total annotated area) was computed in each field of view. Thresholds, hue, and saturation were kept constant for all specimens.

PARPi-FL Staining and Nuclear PARP1 Specificity in Thin Tissue Sections

Fresh discarded BCC tissues were serial-sectioned into four 10-μm frozen sections for PARPi-FL staining, H&E staining, PARP1 immunofluorescence testing, and isotype IgG control (Supplemental Fig. 1A; supplemental materials are available at http://jnm.snmjournals.org). For PARPi-FL staining, tissue sections were stained with 100 nM PARPi-FL (in 30% polyethylene glycol) for 5 min using Hoechst 33342 (Invitrogen), 0.002 mg/mL, as a nuclear counterstain. Immunofluorescence was tested using a previously described procedure (*23*). We used anti-PARP1 antibody (rabbit polyclonal IgG, SC-7150, 1:200 dilution; Santacruz Biotechnology) and isotype control (normal rabbit IgG, 1:200 dilution; Santacruz Biotechnology), and we used AlexaFluor 568 (goat-antirabbit, A21076, 1:1,000 dilution; Invitrogen Molecular Probes) as the secondary antibody. The slides were scanned using a Mirax Slide Scanner (3DHISTECH). For selected tissues, 10–15 PARPi-FL images were also acquired with a commercial microscope (LSM880; Carl Zeiss Microscopy LLC) in tumor and normal areas. Analysis for fluorescence intensity and area positivity on the microscopic images was performed using a batch code implemented in FIJI. Thresholding was performed for PARPi-FL signal, and total nuclear area was calculated using Hoechst 33342 to calculate normalized intensity and area positivity. Analysis was done on an image level and a case level (average of multiple images).

PARPi-FL Staining in Thick Fresh BCC specimens

Specimens were stained with PARPi-FL (250 nM PARPi-FL in 30% polyethylene glycol

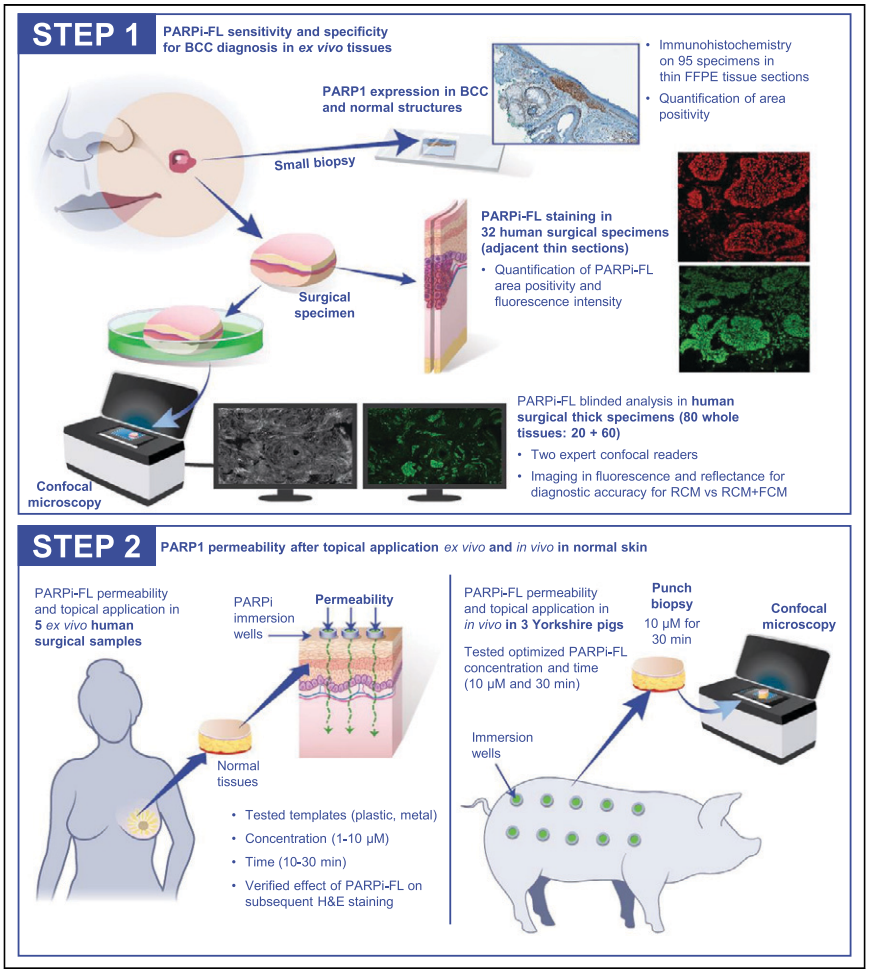

FIGURE 1. Summary of experiments undertaken in study. FFPE = formalin-fixed, paraffin-embedded. FCM = fluorescence confocal microscopy; RCM = reflectance confocal microscopy.

300/phosphate-buffered saline for 10 min, followed by 10 min in 30% polyethylene glycol 300/phosphate-buffered saline) and imaged using a benchtop research ex vivo RCM-and-FCM prototype microscope (Vivascope-2500; Caliber Imaging and Diagnostics) simultaneously in both fluorescence (488 nm) and reflectance (785 nm) modes (Supplemental Fig. 1B). RCM and FCM mosaicking to display up to a 12 × 12 mm field of view encompassing the entire tissue was performed and used for the blinded study.

Blinded Reader Evaluation

The blinded reading study was performed by 2 expert confocal readers. Training was on a subset of RCM and FCM mosaics with an equal number of BCC-positive and BCC-negative cases (i.e., equal prevalence for BCCs and normal skin). Depending on the specimen size, each mosaic was divided into either 2 or 4 submosaics to facilitate reading. The diagnosis was evaluated both at a mosaic (case) level and at an individual submosaic (quadrant) level. Both readers were provided with matched RCM and FCM mosaics for each specimen. The RCM mosaic was evaluated, followed by the matched FCM mosaic to compare BCC diagnostic accuracy on RCM and with added PARPi-FL contrast in RCM and FCM. Readers evaluated BCC presence or absence, nuclear staining (on FCM), and overall diagnostic quality. Blinded analysis results were compared with the corresponding H&E results to compute sensitivity, specificity, positive predictive value, and negative predictive value at a case level and a quadrant level.

Effect of PARPi-FL on Subsequent Histopathology

Normal and BCC tissues were bisected such that one piece was immersed in PARPi-FL (1 μM) and the other in polyethylene glycol–phosphate-buffered saline (control) for 30 min, respectively. Both pieces were separately submitted in formalin for H&E histopathology evaluation. Sections were digitally scanned and read in a blinded manner by 2 pathologists to grade the staining quality of cytoplasm, nucleus, and collagen; diagnostic acceptability or unacceptability; and BCC presence or absence and subtype.

Permeability and Transepidermal Delivery in Ex Vivo Tissue

The mastectomy specimens were processed to remove adipose tissue and blood without disrupting stratum corneum integrity. Tissues were placed on a flat corkboard and gently wiped with an alcohol pad (Webcol alcohol preps; Covidien) and allowed to dry. PARPi-FL was applied topically on the stratum corneum using plastic and metal templates, which served as PARPi-FL reservoirs (Supplemental Fig. 1C). Additionally, in some specimens, a PARPi-FL–saturated gauze (1 μM) followed by a Tegaderm patch (3M Medical) was pinned onto the skin to maintain uniform pressure, to mimic topical application and occlusion in vivo. Ranges of PARPi-FL concentrations (1–10 μM) and application times (10–30 min) were tested. After experiment completion, a 5-mm punch biopsy (MediChoice biopsy punches; Owens and Minor) was performed. Each biopsy sample was bisected and dipped in Hoechst 33342 (Invitrogen) (diluted to 0.002 mg/mL in chilled phosphate-buffered saline) for nuclear counterstaining. The tissues were mounted on their lateral surface for imaging with a confocal microscope (Zeiss LSM880 system [×20/0.8 numerical aperture [NA]]) using 405-nm (Hoechst 33342) and 488-nm (PARPi-FL) wavelengths. The raw files were qualitatively visualized in FIJI.

Permeability and Transepidermal Delivery In Vivo

Topical application and permeability were tested in vivo in adult female Yorkshire pigs obtained under a protocol approved by the institutional animal care and use committee. The pigs were anesthetized using inhalational 5% isoflurane. An area of the flank approximately 46 cm (18 in) in length was selected, shaved, and gently swabbed with ethanol. Any local irritation (confirmed visually) from shaving was allowed to subside before PARPi-FL application. Within this area, 2 sets of rows comprising 5 sites each were marked for the well placement to deliver either PARPi-FL or saline and to perform biopsies (Supplemental Fig. 1D). The application sites were spaced 2 cm apart (edge-to-edge) to prevent cross contamination. Each well (or template) (Everbilt; Home Depot Product Authority, LLC) measured 0.95-cm ($^3/_8$-in) in diameter and was attached to the selected site using an adhesive (Dermabond Advanced; Ethicon US, LLC) in which 1 mL of 10 μM PARPi-FL or saline solution was left for 30 min. Subsequently, ten 8-mm punch biopsies were performed on each pig. The biopsy samples were bisected; one piece was submitted for H&E staining, and the other was promptly imaged using the benchtop ex vivo RCM-and-FCM microscope (Vivascope-2500; Caliber ID). The biopsy samples were processed for histopathology.

Statistical Analysis

Analyses were conducted using Prism (version 8.0; GraphPad), Stata (version 14.2; Stata Corp.), and R (version 2020; R Core Team) with the "rel" package (*29*) to calculate agreement statistics and the "ggplot2" package (*30*) to produce figures. Inferential unpaired-sample comparisons were assessed by the Mann–Whitney *U* test. PARPi-FL intensity and area positivity were converted by a natural log transform because the raw data were right-skewed. Associations of transformed variables with clinical outcomes were analyzed with receiver-operating-characteristic curves. A blinded experiment was conducted to assess diagnostic accuracy using RCM images and RCM-and-FCM images by 2 expert readers. Interrater agreement on the presence of cellular-level features, diagnosis subtyping, and binarized tissue quality assessments was quantified according to Gwet AC1 because of the high marginal imbalance in the sample, in addition to overall percentage agreement. For the effect of PARPi-FL on histopathology, agreement between pathologists was quantified according to Gwet AC1. Statistical significance was determined with an α value of 0.05. Unless stated otherwise, data are presented as mean ± SD, and significance is specified.

RESULTS

PARP1 Expression in BCC and Normal Skin Structures

In 95 specimens, we found PARP1 expression in BCCs (the superficial, nodular, infiltrative, and micronodular subtypes) and in normal structures (Fig. 2A; Supplemental Fig. 2). Higher area positivity was observed in tumors (47.89% ± 21.4), followed by hair follicles, epidermis, and sebaceous glands ($P < 0.001$) (Fig. 2B). The value of 0.927 for area under the curve (AUC) indicates successful discrimination of tumor from normal areas on the basis of PARP1 area positivity (Fig. 2C).

PARPi-FL Staining and PARP1 Immunofluorescence in Thin BCC Sections

In 32 thin BCC sections, PARPi-FL uptake in nuclei correlated with PARP1 expression, confirmed by PARP1 immunofluorescence (Figs. 3A and 3B; Supplemental Figs. 3A and 3B). The fluorescence intensity and area positivity in 394 images (from 32 tissues) demonstrated significantly higher intensity and area positivity in tumors than in normal tissue ($P < 0.01$) with both imagewise and casewise analyses (Fig. 3C; Supplemental Fig. 3C). Similar trends were observed in nontransformed data (Supplemental Figs. 3D and 3E). Area positivity differentiated tumor from normal tissue with higher accuracy (AUC, 0.96) than did fluorescence intensity (AUC, 0.68) (Fig. 3D).

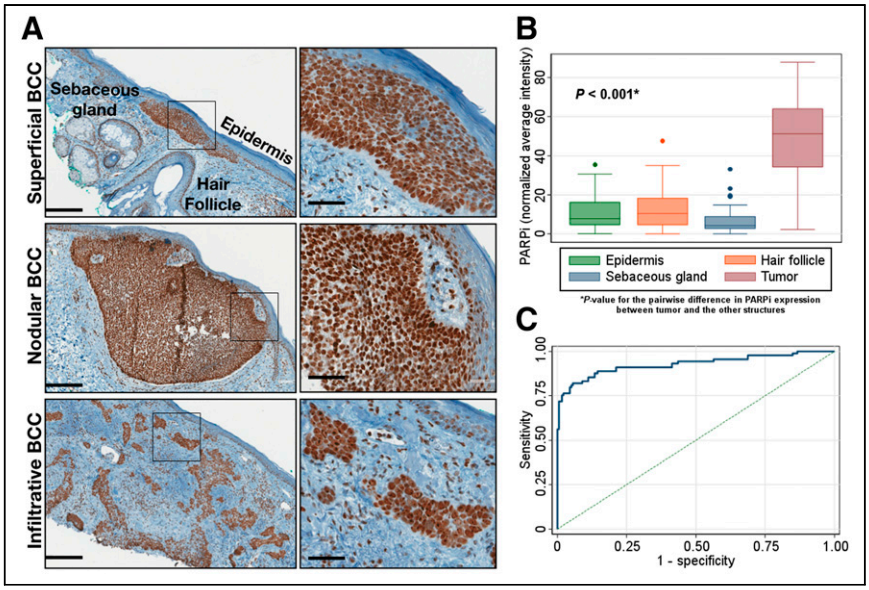

FIGURE 2. Expression of PARP1 is higher in BCCs than in normal skin structures. (A) Representative images of PARP1 expression show high expression in superficial, nodular, and infiltrative BCC, as compared with epidermis, hair follicles, and sebaceous glands. (B) PARP1 area positivity in immunohistochemistry samples ($n = 95$) shows significantly higher positivity in tumors. (C) Receiver-operating-characteristic curve to differentiate tumor from normal skin structures yields AUC of 0.83.

PARPi-FL Staining for Improving BCC Diagnosis in an Ex Vivo Blinded Study

In 83 fresh surgical specimens, PARPi-FL enhanced the visualization of small BCC tumors that otherwise were invisible in the corresponding RCM mosaic, as confirmed on H&E-stained sections (Fig. 4A; Supplemental Fig. 4). Of the 166 RCM and FCM mosaics, 44 were used for training. The blinded evaluation was performed on the remaining 122 mosaics; however, only cases with acceptable diagnostic quality were analyzed. We found higher sensitivity and moderately better specificity in the RCM-and-FCM images than in the RCM-alone images (Figs. 4B and 4C).

Transepidermal Delivery of PARPi-FL Through Intact Skin in Fresh Ex Vivo Human Specimens

In 5 ex vivo normal mastectomy specimens, we tested topical application of PARPi-FL at various concentrations and application times (Fig. 5). We detected PARPi-FL staining in the nuclei of the basal cells of the epidermis and dermal cells, confirming successful permeability. Optimal staining with high nuclear specificity and intensity was observed for the 10 μM PARPi-FL concentration when applied for 30 min. These parameters were selected for in vivo testing in pigs.

Transepidermal Delivery of PARPi-FL in an In Vivo Pig Model

In 3 adult Yorkshire pigs, we verified PARPi-FL permeability in vivo in normal skin after topical application of 10 μM PARPi-FL for 30 min (Fig. 6; Supplemental Fig. 5). Positive nuclear staining in the epidermal basal cell layer was consistently observed in PARPi-FL–treated sites and was absent from the control sites, confirming the permeability and detectability of PARPi-FL after in vivo application. No significant histopathologic differences were noticeable between the PARPi-FL–treated and control groups (Fig. 6; Supplemental Fig. 6).

DISCUSSION

Our results suggest that the addition of exogenous PARPi-FL fluorescence contrast to endogenous reflectance contrast improves noninvasive diagnosis of BCCs. PARP1 proved to be an excellent biomarker; we found consistently higher PARP1 expression in all BCC subtypes than in normal skin structures. Across the 95 specimens investigated, 90% of BCCs had homogeneous PARP1 staining, especially in the superficial and infiltrative subtypes. Some heterogeneous PARP1 expression was observed in a few nodular BCCs (<10%), specifically in the variants with nodular–cystic changes and squamous differentiation (Supplemental Fig. 2E).

We confirmed specific nuclear labeling correlating with PARP1 expression in nucleated tissue areas of tumors, basal epidermal layers in epidermis, hair follicles, and sebaceous glands (Figs. 3A and 3B; Supplemental Figs. 3A and 3B). We used area positivity and intensity parameters to quantitatively confirm PARPi-FL nuclear fluorescence in tumors, as compared with normal nucleated structures—an issue that often confounds BCC diagnosis in vivo. Although both parameters were higher in tumors,

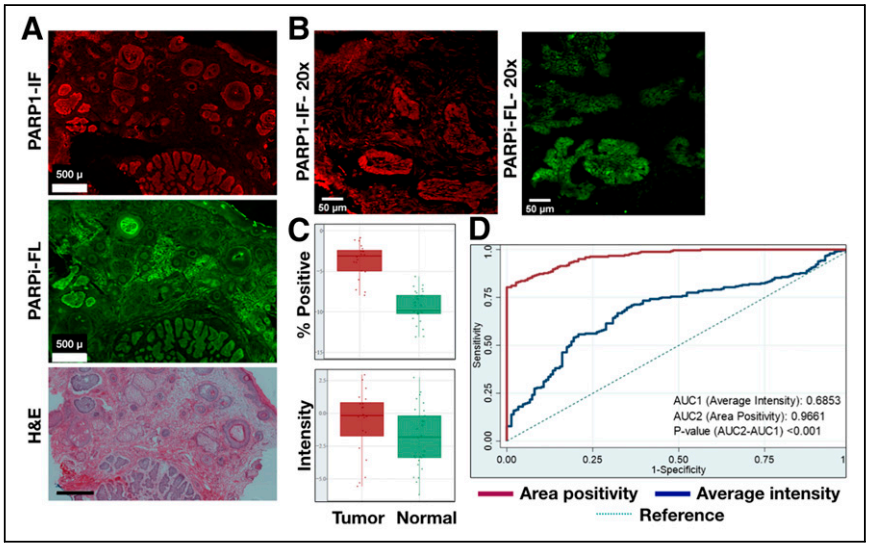

FIGURE 3. Nucleus-specific PARPi-FL staining observed in BCC tissues. (A) Representative images showing successful PARPi-FL nuclear staining in tumor and normal tissue. (B) PARPi-FL nuclear uptake and spatial correlation with nuclear PARP1 in nucleated areas verified in high-resolution images (×20). (C) Higher average intensity and area positivity in tumors than in normal structures in casewise analysis (right) ($P < 0.001$ for percentage area positivity and imagewise intensity). (D) Area positivity better discriminates tumor and normal tissue than does fluorescence intensity (AUC, 0.96 vs. 0.68)

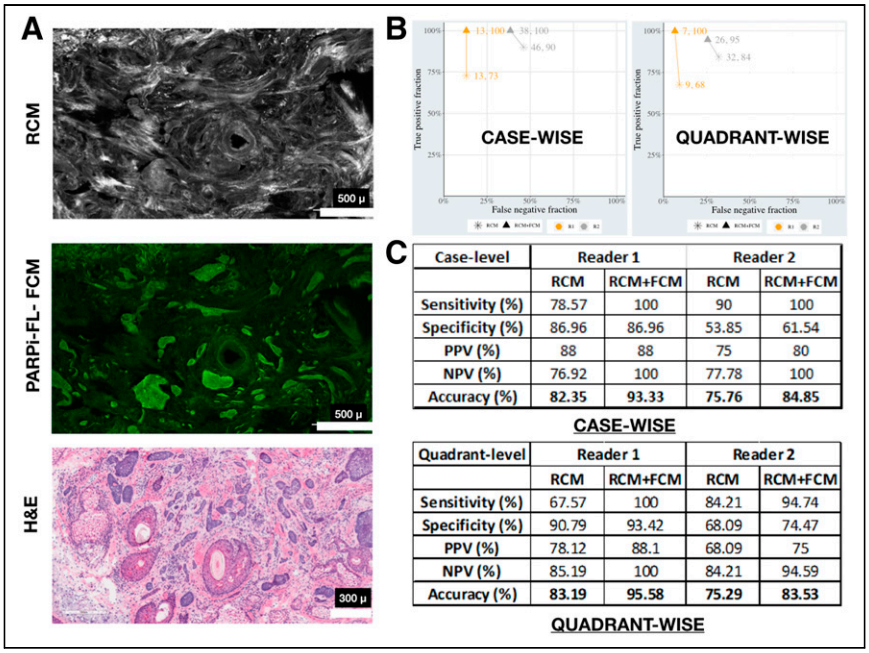

Case-level	Reader 1		Reader 2	
	RCM	RCM+FCM	RCM	RCM+FCM
Sensitivity (%)	78.57	100	90	100
Specificity (%)	86.96	86.96	53.85	61.54
PPV (%)	88	88	75	80
NPV (%)	76.92	100	77.78	100
Accuracy (%)	82.35	93.33	75.76	84.85

CASE-WISE

Quadrant-level	Reader 1		Reader 2	
	RCM	RCM+FCM	RCM	RCM+FCM
Sensitivity (%)	67.57	100	84.21	94.74
Specificity (%)	90.79	93.42	68.09	74.47
PPV (%)	78.12	88.1	68.09	75
NPV (%)	85.19	100	84.21	94.59
Accuracy (%)	83.19	95.58	75.29	83.53

QUADRANT-WISE

FIGURE 4. PARPi-FL contrast in FCM images improves BCC diagnostic accuracy over RCM alone. (A) PARPi-FL contrast improves visualization of BCCs, as compared with RCM alone, as confirmed on H&E images. (B and C) Higher sensitivity in RCM-and-FCM images and moderate increase in specificity found in blinded evaluation in both casewise and quadrantwise analysis. NPV = negative predictive value; PPV = positive predictive value.

only area positivity could successfully differentiate tumor from normal structures with a high accuracy (Fig. 3D). We acknowledge that none of these parameters would have utility in clinical practice (as Hoechst 33342 or other nuclear dyes cannot be applied on patients); however, PARPi-FL staining would enhance the cellular and morphologic details that help aid an expert RCM reader to differentiate BCCs from normal structures and improve the diagnosis. This improvement was also demonstrated through the blinded analysis performed by 2 expert RCM readers—an analysis in which PARPi-FL contrast, when combined with RCM, boosted the diagnostic accuracy, as compared with RCM alone. In general, nuclear staining was observed in most tissues; only 5 of 62 (8%) tissues had minimal or no nuclear staining in tumor or normal structures. This finding was in contrast to PARP1 expression, with only 1.1% of specimens showing low or negative expression. A higher rate of inconsistent nuclear staining could be attributed to the delays in fresh tissue handling, since PARP1 can rapidly degrade in excised tissues. Despite some heterogeneity in PARPi-FL nuclear labeling, we demonstrated that a combined imaging approach (RCM and FCM) improved diagnostic performance, especially sensitivity, when compared with RCM alone. Surprisingly, we found minimal improvements in specificity in the blinded study. False-positives were more prevalent in cases with smudged PARPi-FL staining, possibly attributable to the variability in tissue quality. Furthermore, ex vivo tissues do not image as well as skin in vivo (*31–33*), probably because of tissue dehydration and alterations in refractive index and optical properties. Differences in the training of the 2 readers may have impacted improvements in sensitivity and specificity. We do not anticipate these tissue-related issues during in vivo imaging in patients (our ultimate goal). Thus, we expect better results, in terms of both higher sensitivity and higher specificity, with use of RCM-and-FCM imaging, when performed in patients through a clinical trial.

The next critical issue that makes a contrast agent suitable for topical application is permeability through intact skin. We successfully demonstrated that PARPi-FL can passively diffuse through the stratum corneum after topical application in ex vivo human tissues and in vivo pig skin. Skin is characterized by a tightly and coordinately regulated molecular transport system, which allows molecules with low molecular weight (<500 Da) and lipophilicity (logP, 1–3) to permeate the stratum corneum. Thus, the borderline molecular weight and lipophilicity of PARPi-FL (620 Da; logP, 2.9) makes it suitable for topical application and transepidermal delivery. We found that PARPi-FL at a 10 μM concentration and 30 min yielded consistent labeling in nucleated cells throughout the epidermis into the dermis in human and pig tissues. To deliver the dye, we attached reservoirs to the skin; however, this delivery approach would not be feasible in patients. Thus, to demonstrate clinical feasibility, we also tested PARPi-FL permeability and detectability using a saturated gauze (mimicking a nicotine patch) applied to the skin under occlusion, which yielded similar results (Supplemental Fig. 5), laying the foundation for developing a cream- or gel-based formulation for topical application in clinics. Furthermore, PARPi-FL application to the skin did not influence the subsequent H&E staining of tissue (Supplemental Fig. 6).

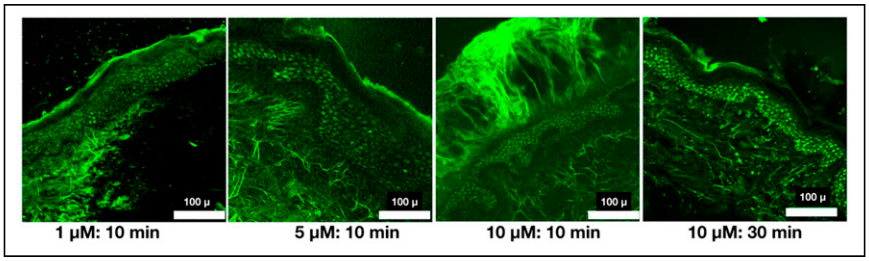

FIGURE 5. PARPi-FL successfully permeates through intact skin in ex vivo human tissue. Increased nuclear labeling is found for longer periods; maximum labeling and intensity are found for 10 μM and 30 min.

CONCLUSION

Higher PARP1 expression was found in BCCs than in normal skin structures, allowing specific PARPi-FL labeling in BCCs. Enhanced contrast provided by PARPi-FL–labeled nuclei leads to higher sensitivity and specificity for BCC diagnosis with RCM-and-FCM imaging than for RCM imaging alone. PARPi-FL can be delivered

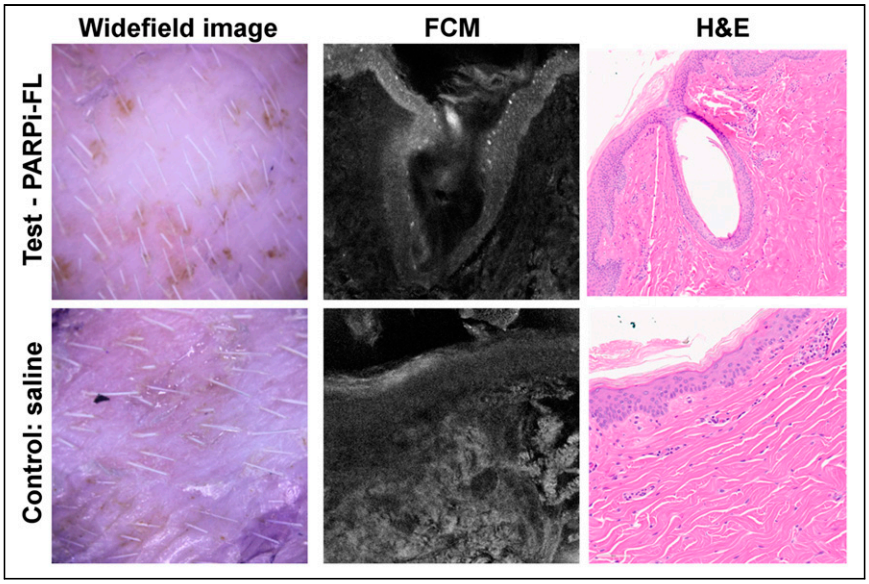

FIGURE 6. Successful PARPi-FL staining confirmed in vivo after topical application in live pig model. Representative wide-field, FCM, and H&E images demonstrate positive nuclear staining in basal layer of epidermis in test image (PARPi-FL), with absence of nuclear labeling in control image.

KEY POINTS

QUESTION: Can PARPi-FL combined with reflectance contrast improve detection of BCCs?

PERTINENT FINDINGS: Higher PARP1 expression and PARPi-FL staining were confirmed in nuclei of tumor cells than in normal skin structures. In a blinded study by 2 readers, diagnostic accuracy for BCCs was higher for combined PARPi-FL and reflectance contrast than for reflectance contrast alone. The permeability of PARPi-FL through passive diffusion was also confirmed in human skin and in vivo in pigs.

IMPLICATIONS FOR PATIENT CARE: Improving noninvasive diagnosis will directly impact clinical care and management of BCCs by reducing benign biopsies and enabling nonsurgical management of less aggressive BCC subtypes.

into the dermis (1–10 μM, 10–30 min) after passive topical application, suggesting promising potential for clinical use in patients. However, staining was found to be heterogeneous in 8% of thick specimens, suggesting that a combination of FCM with RCM may be necessary for improving clinical diagnosis of BCCs in vivo in patients.

DISCLOSURE

This work was supported by National Institutes of Health grants P30 CA008748, R01 EB020029 (Milind Rajadhyaksha), and R01 CA204441 (Thomas Reiner); the MSK Imaging and Radiation Sciences Program; and the MSK Society Grant (Manu Jain). Thomas Reiner, Susanne Kossatz, and Christian Brand are shareholders of Summit Biomedical Imaging, LLC. Thomas Reiner and Susanne Kossatz are coinventors on a filed U.S. patent (WO2016164771) held by MSK that covers methods for PARPi-FL. Thomas Reiner is a coinventor on a U.S. patent (WO2012074840), held by the General Hospital Corporation, that covers PARPi-FL composition. Thomas Reiner is a paid consultant for Theragnostics, Inc. Christian Brand serves as the chief scientific officer at Summit Biomedical Imaging, LLC. Christi Alessi-Fox is a former employee of, holds equity in, and is currently a consultant with Caliber Imaging and Diagnostics. Milind Rajadhyaksha is a former employee of and owns equity in Caliber Imaging and Diagnostics; the VivaScope is the commercial version of an original laboratory prototype that he developed at Massachusetts General Hospital, Harvard Medical School. No other potential conflict of interest relevant to this article was reported.

ACKNOWLEDGMENTS

We acknowledge Dr. Evan Matros and the PPBC team, Brandon Possum and the Mohs Lab, Eric Chan and the MCCF Core, the MSK–Animal Imaging Core Facility, the Radiochemistry and Molecular Imaging Probes Core, the Nuclear Magnetic Analytical Core, and the MSK Center for Molecular Imaging and Nanotechnology.

REFERENCES

1. Rogers HW, Weinstock MA, Feldman SR, Coldiron BM. Incidence estimate of nonmelanoma skin cancer (keratinocyte carcinomas) in the U.S. population, 2012. *JAMA Dermatol.* 2015;151:1081–1086.
2. Work Group; Invited Reviewers, Kim JYS, Kozlow JH, Mittal B, Moyer J, Olencki T, Rodgers P. Guidelines of care for the management of basal cell carcinoma. *J Am Acad Dermatol.* 2018;78:540–559.
3. Wozniak-Rito A, Zalaudek I, Rudnicka L. Dermoscopy of basal cell carcinoma. *Clin Exp Dermatol.* 2018;43:241–247.
4. Reiter O, Mimouni I, Gdalevich M, et al. The diagnostic accuracy of dermoscopy for basal cell carcinoma: a systematic review and meta-analysis. *J Am Acad Dermatol.* 2019;80:1380–1388.
5. Altamura D, Menzies SW, Argenziano G, et al. Dermatoscopy of basal cell carcinoma: morphologic variability of global and local features and accuracy of diagnosis. *J Am Acad Dermatol.* 2010;62:67–75.
6. Dinnes J, Deeks JJ, Chuchu N, et al. Visual inspection and dermoscopy, alone or in combination, for diagnosing keratinocyte skin cancers in adults. *Cochrane Database Syst Rev.* 2018;12:CD011901.
7. Rajadhyaksha M, Grossman M, Esterowitz D, Webb RH, Anderson RR. In vivo confocal scanning laser microscopy of human skin: melanin provides strong contrast. *J Invest Dermatol.* 1995;104:946–952.
8. Rajadhyaksha M, González S, Zavislan JM, Anderson RR, Webb RH. In vivo confocal scanning laser microscopy of human skin II: advances in instrumentation and comparison with histology. *J Invest Dermatol.* 1999;113:293–303.
9. Rajadhyaksha M, Anderson RR, Webb RH. Video-rate confocal scanning laser microscope for imaging human tissues in vivo. *Appl Opt.* 1999;38:2105–2115.
10. Guitera P, Menzies S, Argenziano G, et al. Dermoscopy and in vivo confocal microscopy are complementary techniques for diagnosis of difficult amelanotic and light-coloured skin lesions. *Br J Dermatol.* 2016;175:1311–1319.
11. Ruini C, Hartmann D, Saral S, Krammer S, Ruzicka T, von Braunmühl T. The invisible basal cell carcinoma: how reflectance confocal microscopy improves the diagnostic accuracy of clinically unclear facial macules and papules. *Lasers Med Sci.* 2016;31:1727–1732.
12. Nelson SA, Scope A, Rishpon A, et al. Accuracy and confidence in the clinical diagnosis of basal cell cancer using dermoscopy and reflex confocal microscopy. *Int J Dermatol.* 2016;55:1351–1356.
13. Liopyris K, Navarrete-Dechent C, Yélamos O, Marchetti M, Rabinovitz H, Marghoob A. Clinical, dermoscopic and reflectance confocal microscopy characterization of facial basal cell carcinomas presenting as small white lesions on sun-damaged skin. *Br J Dermatol.* 2019;180:229–230.
14. Dinnes J, Deeks JJ, Saleh D, et al. Reflectance confocal microscopy for diagnosing cutaneous melanoma in adults. *Cochrane Database Syst Rev.* 2018;12:CD013190.

15. Lupu M, Popa IM, Voiculescu VM, et al. A retrospective study of the diagnostic accuracy of in vivo reflectance confocal microscopy for basal cell carcinoma diagnosis and subtyping. *J Clin Med.* 2019;8:449.
16. Jain M, Pulijal SV, Rajadhyaksha M, Halpern AC, Gonzalez S. Evaluation of bedside diagnostic accuracy, learning curve, and challenges for a novice reflectance confocal microscopy reader for skin cancer detection in vivo. *JAMA Dermatol.* 2018;154:962–965.
17. Witkowski AM, Łudzik J, DeCarvalho N, et al. Non-invasive diagnosis of pink basal cell carcinoma: how much can we rely on dermoscopy and reflectance confocal microscopy? *Skin Res Technol.* 2016;22:230–237.
18. Xiong Y-Q, Ma S-J, Mo Y, Huo S-T, Wen Y-Q, Chen Q. Comparison of dermoscopy and reflectance confocal microscopy for the diagnosis of malignant skin tumours: a meta-analysis. *J Cancer Res Clin Oncol.* 2017;143:1627–1635.
19. Witkowski AM, Łudzik J, Arginelli F, et al. Improving diagnostic sensitivity of combined dermoscopy and reflectance confocal microscopy imaging through double reader concordance evaluation in telemedicine settings: a retrospective study of 1000 equivocal cases. *PLoS One.* 2017;12:e0187748.
20. Rajadhyaksha M, Gonzalez S, Zavislan JM. Detectability of contrast agents for confocal reflectance imaging of skin and microcirculation. *J Biomed Opt.* 2004;9:323–331.
21. Reiner T, Lacy J, Keliher EJ, et al. Imaging therapeutic PARP inhibition in vivo through bioorthogonally developed companion imaging agents. *Neoplasia.* 2012;14:169–177.
22. Carney B, Kossatz S, Lok BH, et al. Target engagement imaging of PARP inhibitors in small-cell lung cancer. *Nat Commun.* 2018;9:176.
23. Kossatz S, Brand C, Gutiontov S, et al. Detection and delineation of oral cancer with a PARP1 targeted optical imaging agent. *Sci Rep.* 2016;6:21371.
24. Irwin CP, Portorreal Y, Brand C, et al. PARPi-FL-a fluorescent PARP1 inhibitor for glioblastoma imaging. *Neoplasia.* 2014;16:432–440.
25. Kossatz S, Pirovano G, França PDDS, et al. Validation of the use of a fluorescent PARP1 inhibitor for the detection of oral, oropharyngeal and oesophageal epithelial cancers. *Nat Biomed Eng.* 2020;4:272–285.
26. de Souza França PD, Kossatz S, Brand C, et al. A phase I study of a PARP1-targeted topical fluorophore for the detection of oral cancer. medRxiv website. https://www.medrxiv.org/content/10.1101/2020.11.09.20228536v1.full. Published November 12, 2020. Accessed January 31, 2022.
27. Thurber GM, Yang KS, Reiner T, et al. Single-cell and subcellular pharmacokinetic imaging allows insight into drug action in vivo. *Nat Commun.* 2013;4:1504.
28. Olson AH. *Image Analysis Using the Aperio ScanScope.* Aperio Technologies Inc.; 2006.
29. LoMartire R, LoMartire MR. Package rel: reliability coefficients. R Package Documentation website. https://rdrr.io/cran/rel/. Accessed February 23, 2022.
30. Wickham H, Chang W, Wickham MH. Package 'ggplot2'. Create elegant data visualisations using the grammar of graphics. Version 2(1). 2016. The Comprehensive R Archive Network (CRAN) website. https://cran.r-project.org/web/packages/ggplot2/ggplot2.pdf. Accessed February 23, 2022.
31. Rajadhyaksha M, Menaker G, Flotte T, Dwyer PJ, González S. Confocal examination of nonmelanoma cancers in thick skin excisions to potentially guide Mohs micrographic surgery without frozen histopathology. *J Invest Dermatol.* 2001;117:1137–1143.
32. Patel YG, Nehal KS, Aranda I, Li Y, Halpern AC, Rajadhyaksha M. Confocal reflectance mosaicing of basal cell carcinomas in Mohs surgical skin excisions. *J Biomed Opt.* 2007;12:034027.
33. Gareau DS, Patel Y, Li Y, et al. Confocal mosaicing microscopy in skin excisions: a demonstration of rapid surgical pathology. *J Microsc.* 2009;233:149–159.